Nonpercolative nature of the metal-insulator transition and persistence of local Jahn-Teller distortions in the rhombohedral regime of $La_{1-x}Ca_xMnO_3$

Mouath Shatnawi
Department of Physics, The Hashemite University, Zarqa 13115, Jordan

Emil S. Bozin*
Department of Condensed Matter Physics and Materials Science, Brookhaven National Laboratory, Upton, New York 11973, USA

J. F. Mitchell
Materials Science Division, Argonne National Laboratory, Argonne, Illinois 60439, USA

Simon J. L. Billinge
Department of Condensed Matter Physics and Materials Science, Brookhaven National Laboratory, Upton, New York 11973, USA
and Department of Applied Physics and Applied Mathematics, Columbia University, New York, New York 10027, USA

(Received 25 November 2015; revised manuscript received 13 April 2016; published 25 April 2016)

Evolution of the average and local crystal structure of Ca-doped $LaMnO_3$ has been studied across the metal to insulator (MI) and the orthorhombic to rhombohedral (OR) structural phase transitions over a broad temperature range for two Ca concentrations ($x = 0.18, 0.22$). Combined Rietveld and high real space resolution atomic pair distribution function (PDF) analysis of neutron total scattering data was carried out with aims of exploring the possibility of nanoscale phase separation (PS) in relation to MI transition, and charting the evolution of local Jahn-Teller (JT) distortion of MnO_6 octahedra across the OR transition at $T_S \sim 720$ K. The study utilized explicit two-phase PDF structural modeling, revealing that away from T_{MI} there is no evidence for nanoscale phase coexistence. The local JT distortions disappear abruptly upon crossing into the metallic regime both with doping and temperature, with only a small temperature-independent signature of quenched disorder being observable at low temperature as compared to $CaMnO_3$. The results hence do not support the percolative scenario for the MI transition in $La_{1-x}Ca_xMnO_3$ based on PS, and question its ubiquity in the manganites. In contrast to $LaMnO_3$ that exhibits long-range orbital correlations and sizable octahedral distortions at low temperature, the doped samples with compositions straddling the MI boundary exhibit correlations (in the insulating regime) limited to only $\sim$1 nm with observably smaller distortions. In the $x = 0.22$ sample local JT distortions are found to persist across the OR transition and deep into the R phase (up to $\sim$1050 K), where they are crystallographically prohibited. Their magnitude and subnanometer spatial extent remain unchanged.

DOI: 10.1103/PhysRevB.93.165138

I. INTRODUCTION

Manganites, such as the perovskite structured calcium doped lanthanum manganite $La_{1-x}Ca_xMnO_3$ (LCMO), are considered as a model system for studying the response of materials to the presence of competing interactions [1–5], yet despite extensive study the emergent properties, such as the colossal magnetoresistance (CMR) and the metal-insulator (MI) transition, in these materials are far from well understood.

Much recent work has focused on an inhomogeneous, or what is called phase separation (PS), picture [6–13] where metallic domains are assumed to form in an insulating background and the MI transition proceeds via a percolative mechanism where the metallic cluster size increases as the MI transition is approached resulting in a conducting path extending from one side of the sample to the other. Although the PS picture has been supported by many experimental studies such as scanning tunneling spectroscopy [14], small angle neutron scattering [15], atomic pair distribution function (PDF) [16], and nuclear magnetic resonance [17], there are some experimental results that are better explained based on the homogeneous picture [18–21] and the issue needs a more careful assessment.

Through the strong electron-lattice interaction, the presence or absence of a JT distortion has been shown to be a sensitive indicator of the electronic state of the material, insulating or metallic [22]. It manifests itself in the MnO bond length ($r_{Mn\text{-}O}$) distribution in the MnO_6 octahedron, irrespective of whether the distortions are long-range ordered or not [23,24]. When the JT distortion is present, the distribution of near neighbor $r_{Mn\text{-}O}$ distances constituting the MnO_6 octahedron will consist of two long ($\sim$2.16 Å in $LaMnO_3$ endmember), two intermediate, and two short (<2 Å) Mn-O bonds [Fig. 1(a)]. When the JT distortion is absent there are six equal $r_{Mn\text{-}O}$ distances on the octahedron [Fig. 1(b)]. Observation of the JT distortion in probes of local structure are associated with the insulating phase [22,25,26], whereas deep in the metallic regime at base temperature no appreciable signature of the JT distortions have been observed on any length scale [26].

Here we apply the PDF method to study structural changes in $La_{1-x}Ca_xMnO_3$ as a function of temperature for two carefully chosen concentrations: $x = 0.18$ and $x = 0.22$. These two concentrations straddle the doping-induced MI

*Corresponding author: bozin@bnl.gov

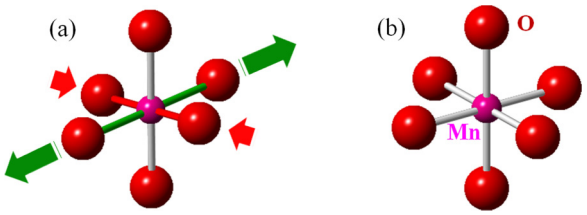

FIG. 1. MnO_6 octahedra—basic building block of the $La_{1-x}Ca_xMnO_3$ structure: (a) JT distorted, with pairs of long (green), intermediate (gray), and short (red) Mn-O distances; (b) undistorted, with all Mn-O distances equal (gray).

transition, enabling us to cross the MI transition both as a function of doping and temperature. For $x = 0.18$ the system exhibits insulating behavior at all temperatures. For $x = 0.22$, at low temperatures the system is ferromagnetic metallic (FM). By heating to temperatures above ~180 K it becomes a paramagnetic insulator (PI). The key result is that local JT distortions disappear abruptly at the MI transition both as a function of doping at fixed temperature, and by temperature at fixed doping. Explicit two-phase modeling reveals no evidence of phase coexistence away from T_{MI}. This is incompatible with a percolative picture of the phase transition.

Additionally, we have studied the transition to the high temperature rhombohedral phase on heating in the $x = 0.22$ material. Local JT distortions persist at high temperature, although they are crystallographically prohibited in the $R\bar{3}c$ phase, similar to the earlier observation in the $LaMnO_3$ endmember [23,27]. Transition to the rhombohedral regime appears rather continuous from the local structure perspective, with no observable change in the size and spatial extent of the local distortions.

II. EXPERIMENT AND MODELING

Finely pulverized samples of $La_{1-x}Ca_xMnO_3$ with two compositions, $x = 0.18$ and $x = 0.22$, were prepared using standard solid state synthesis methods [23], annealed to ensure oxygen stoichiometry [28], and characterized thoroughly [26]. Neutron powder diffraction measurements were carried out at the NPDF diffractometer at Los Alamos Neutron Scattering Center at Los Alamos National Laboratory. The samples, approximately 6 g each, were loaded into extruded vanadium containers and sealed under He atmosphere. The data were collected on warming for both samples at various temperatures between 10 and 550 K using a closed cycle cryo-furnace. In addition, in order to explore the atomic structure at various length scales within the high temperature rhombohedral phase, data on the $x = 0.22$ sample were also collected on warming in the ILL furnace up to a temperature of 1050 K. Transformation to rhombohedral phase for this composition occurs at ~720 K [29]. Control furnace measurement at 550 K was conducted on cooling to ensure the sample integrity. Data were collected for 4 h at each temperature on each sample, providing good statistics and a favorable signal to noise ratio at high momentum transfers. Raw data were normalized and various experimental corrections performed following standard reduction protocols [30]. High resolution experimental PDFs were obtained from the sine Fourier transform of the measured total scattering structure functions $F(Q)$ over a broad range of momentum transfers up to $Q_{max} = 35\ \text{Å}^{-1}$. Data reduction to obtain the PDFs, $G(r)$, was carried out using the program PDFGETN [31].

The average structure was assessed through the Rietveld refinements [32] to the raw diffraction data using GSAS [33] operated under EXPGUI [34]. Structural refinements of the PDF data were carried out over $1.7 < r < 3.5$ Å range using PDFFIT2 operated under PDFGUI [35]. In addition, for PDF data at selected temperatures refinements were also carried out using a variable r_{max} protocol [23]. In this, the low-r refinement bound was kept fixed at 1.7 Å, while the upper-r bound was systematically changed from 3.5 to 20 Å to provide an estimate of the correlation length of the locally ordered distortions.

The average structure refinements were carried out by the known structural models appropriate for the temperature and concentration ranges used. The O' structural model ($Pnma$) was used for temperatures up to 650 K [36] and the R structural model ($R\bar{3}c$) was used for the 750–1050 K range [37,38]. The local and intermediate structure refinements of PDF data for all temperatures were carried out with O' structural model. All refinements were carried out with isotropic atomic displacement parameters (ADP). Two-phase refinements were carried out to explore the phase separation scenario: both phases were described within the O' structure, with structural parameters fixed to values obtained deep in the metallic and insulating regimes, and only parameters allowed to vary were the phase fraction and the atomic ADPs. The later were constrained to be the same for related atomic sites across the two phases.

III. RESULTS AND DISCUSSION

A. Structural evolution across the MI transition from single phase modeling

1. Average and local structure

First, we briefly review the behavior of Mn-O bond lengths and isotropic ADPs of oxygen when modeled using a single phase model that was previously described and reported in earlier work [26].

Figure 2 summarizes the situation from the average structure perspective (Rietveld refinement). At these compositions in the 10–300 K temperature range the samples show a very small, or negligible [25,29,39–41], JT distortion with all six Mn-O bonds in the octrahedra having a similar length in the range around 1.975 Å. For reference, the Mn-O bonds in the undoped endmember, where the JT distorted octahedra are long-range ordered, are 2.16, 1.96, and 1.93 Å, as shown in the figure as the dashed lines. On the other hand, an enlarged ADP of oxygen on the octahedra indicates that there is some disorder associated with the oxygen positions, consistent with the presence of disordered JT distorted octahedra (for comparison the isotropic ADP of the same oxygen site when no structural disorder is present, in the $CaMnO_3$ endmember [36], is shown as the dashed line) [42]. The value of the oxygen ADP rapidly decreases in the $x = 0.22$ sample as it enters the metallic phase at low temperature, approaching, but not reaching, the undistorted value [Fig. 2(d)]. The slightly enhanced value of this ADP at base temperature is presumably a signature of the quenched disorder component due to Ca/La

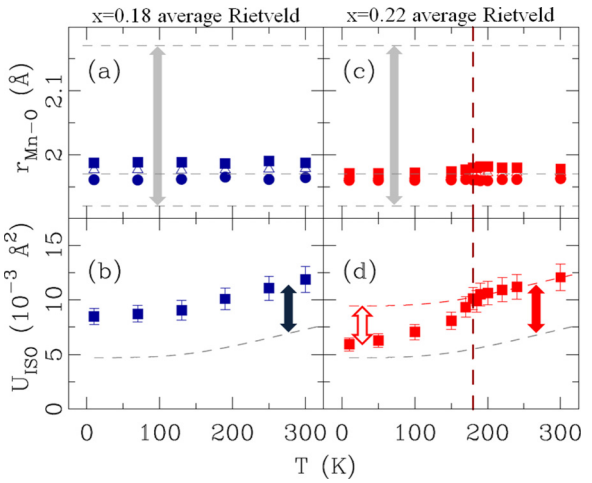

FIG. 2. Average structure behavior (Rietveld). Top row: Temperature evolution of the average Mn-O distances of MnO_6 octahedron for (a) $x = 0.18$ (blue symbols) and (c) $x = 0.22$ (red symbols). Horizontal dashed lines represent these distances in $LaMnO_3$ endmember with vertical gray double arrows indicating the distortion size. Bottom row: Temperature evolution of uncorrelated isotropic atomic displacement parameter (ADP) of 8*d* oxygen (*Pnma* model) for (b) $x = 0.18$ (blue symbols) and (d) $x = 0.22$ (red symbols). Sloping dashed gray lines denote uncorrelated isotropic ADPs of the same oxygen site in $CaMnO_3$ endmember as a reference in the absence of disorder [36]. Sloping dashed red line in (d) represents the same, but with added constant offset to match the high temperature end of the ADP data. Double arrows indicate excess disorder in doped samples as compared to $CaMnO_3$. The vertical dashed red line marks T_{MI}.

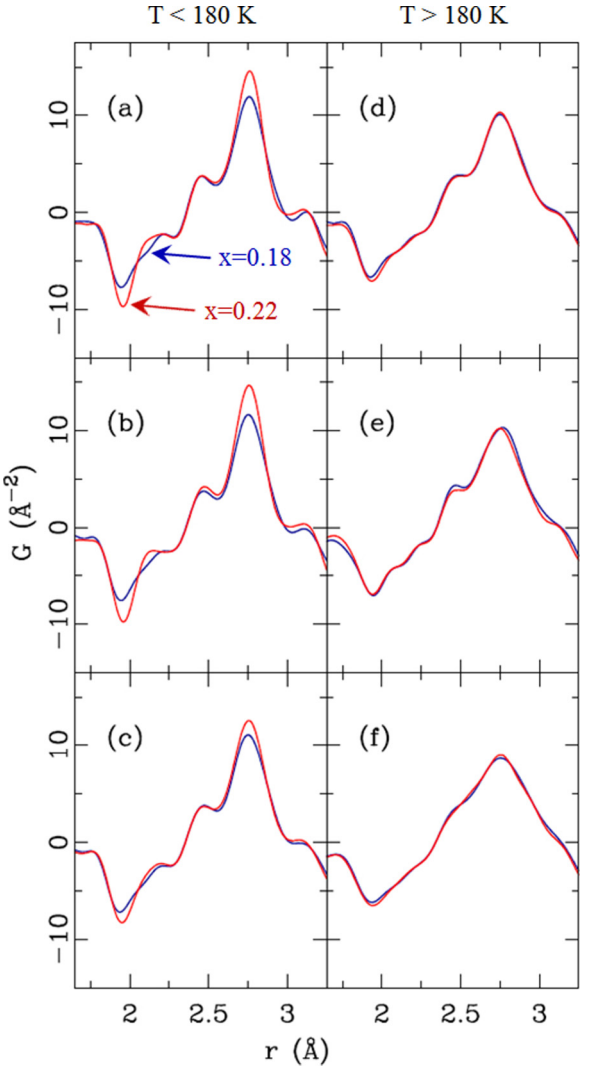

FIG. 3. Comparison of experimental PDFs over *r* range describing MnO_6 octahedron, for $x = 0.18$ (solid blue line) and $x = 0.22$ (solid red line) at various comparable temperatures: $T < T_{MI}$ (left column), and $T > T_{MI}$ (right column). (a) 10 K, (b) ~50 K, (c) ~150 K, (d) ~250 K (e) 300 K, and (f) 550 K. Notable difference can be observed at low temperature where the $x = 0.18$ sample is insulating, whereas the $x = 0.22$ sample is metallic. At $T > T_{MI}$ visible difference vanishes.

substitution, which is a temperature independent quantity. Refinements of the PDF over a range $1.7 < r < 40$ Å (not shown) quantitatively agrees with the Rietveld results.

Examination of the measured PDFs in the low-*r* region of the data confirm that the enlarged ADPs seen in Rietveld are coming from the presence of non-long-range-ordered JT distorted octahedra. This is most effectively demonstrated by comparison between the experimental PDFs when the PDF profiles of the two concentrations are plotted on top of each other, as shown in Fig. 3. For temperatures lower than T_{MI} [Figs. 3(a)–3(c)] the PDFs for the two samples show different features. For higher temperatures [Figs. 3(d)–3(f)] the PDFs of $x = 0.18$ and $x = 0.22$ are very similar. For both samples and at all measured temperatures the PDF peak corresponding to the Mn-O bonds on the MnO_6 octahedra can be seen around 2 Å. This appears upside down, as a negative peak, due to the negative scattering length of Mn [30]. Furthermore, the compound peak at around 2.75 Å includes the O-O distances on the octahedron [36]. The first PDF peak for $x = 0.18$ and for all measured temperatures exhibits a shoulder on the high *r* side of the peak. Since at low temperatures the thermal broadening effect will be minor, the appearance of this shoulder indicates the existence of a longer Mn-O bond, and therefore the presence of a JT distortion. For $x = 0.22$ below 180 K (MI transition temperature) the Mn-O peak appears as a single, well defined, peak. Additionally, the compound peak describing O-O distances on the MnO_6 octahedron is sharp for $x = 0.22$ (undistorted MnO_6) and broad for $x = 0.18$ (distorted MnO_6). These structural features may be used to monitor changes in the JT content as the sample passes through the MI transition. As the measurement temperature of the $x = 0.22$ sample is increased above 180 K a shoulder starts to appear on the high-*r* side similar to the one seen in $x = 0.18$ sample coinciding with the MI transition observed in transport [26]. This was previously pointed out in the context of a temperature dependent study in $La_{1-x}Ca_xMnO_3$ [22] but we show that the effect is similarly seen when the MI transition is crossed as a function of doping at constant temperature.

Quantitative analysis from PDF refinements carried out over a narrow *r* range, reveal the distribution of bond lengths within the local JT distorted octahedra [Figs. 4(a) and 4(c)], with ADPs of 8*d*-O associated with these fits shown in

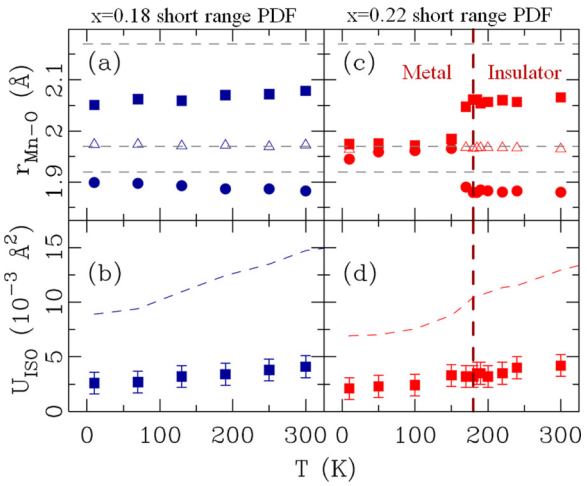

FIG. 4. Local structure behavior (PDF). Top row: Temperature evolution of the local Mn-O distances of MnO_6 octahedron for (a) $x = 0.18$ (blue symbols) and (c) $x = 0.22$ (red symbols). Horizontal dashed lines represent these distances in $LaMnO_3$ endmember. Bottom row: Temperature evolution of correlated isotropic ADPs of 8*d* oxygen (*Pnma* model) for (b) $x = 0.18$ (blue symbols) and (d) $x = 0.22$ (red symbols). Dashed lines sketch the uncorrelated ADPs shown in Figs. 2(b) and 2(d) for reference. The vertical dashed red line marks T_{MI}.

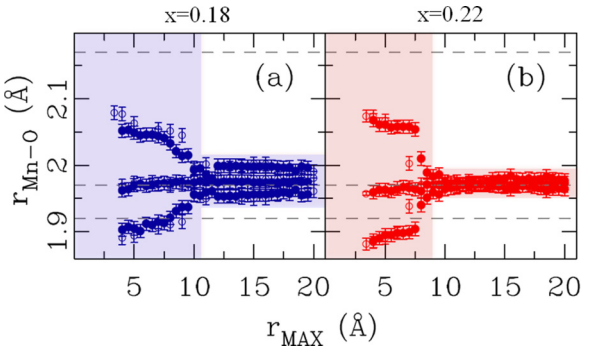

FIG. 5. Mn-O bond lengths from the refined structure model to PDF data as a function of upper refinement limit r_{max} for (a) $x = 0.18$ and (b) $x = 0.22$ compositions. Assessment for $x = 0.18$ was done at 10 K (solid symbols) and 300 K (open symbols), whereas for $x = 0.22$ at 300 K for PDF data obtained at Q_{max} values of 25 Å^{-1} (open symbols) and 35 Å^{-1} (solid symbols). Dashed lines indicate Mn-O bond lengths in $LaMnO_3$ at 300 K, where octahedral distortions are long-range ordered. See text for details.

Figs. 4(b) and 4(d). The latter show no anomalies at the MI transition temperature since all the information about the local distortions has been captured by the structure parameters rather than the ADPs [26].

These observations reinforce the well known result that the MI transition is accompanied by the formation of local JT distortions in the insulating phase, and, conversely, undistorted octahedra in the metallic regime. It also demonstrates that the local bond-length distribution in the insulating regime decreases in amplitude with increasing Ca content, as opposed to the assumption of the small polaron picture in which the local octahedral distortion is as large as in the $LaMnO_3$ endmember [16,43,44] associated with the charge localized Mn^{3+} sites, while Mn^{4+} sites are undistorted as in $CaMnO_3$.

2. *Correlation length of local JT distortions*

The PDF yields the structure on different length scales, revealing the locally JT distorted octahedra at low r and the average, undistorted, structure at high r. By studying how the PDF signal crosses over from the distorted to undistorted as a function of r we may extract a correlation length for any local ordering of the JT distorted octahedra. A variable range PDF refinement of the 300 K data was performed from $r_{min} = 1.7$ Å to r_{max}, where r_{max} was increased from 3.5 to 20 Å in steps of 0.5 Å. The r_{Mn-O} bond lengths extracted from these refinements are shown in Fig. 5. It can be seen that the amplitude of the measured octahedral distortion falls off gradually with increased fitting range until the r_{Mn-O} distances reach the values from the crystallographic analysis. The correlation length of the local JT distortions is ~10.5 Å at $x = 0.18$, decreasing to ~8 Å at $x = 0.22$. This is very similar to the observation above the JT transition in $LaMnO_3$ [23], albeit the length scale in the present case appears to be smaller, suggesting the decrease of the local distortion correlation length with Ca doping.

We have tested whether the length scale of ordered local distortions changes with temperature for the $x = 0.18$ sample. Figure 5(a) shows results of the assessment at 10 and 300 K and we could not detect a temperature evolution of the characteristic length scale within the accuracy of the approach. We also tested whether the observations are dependent on the r resolution of the PDF for $x = 0.22$ by doing the analysis from PDFs obtained using Q_{max} values of 25 and 35 Å^{-1} [open and solid symbols, respectively, in Fig. 5(b)]. We find that slightly sharper and larger length scale (by ~1 Å) is obtained with higher resolution data, giving us an estimate of the uncertainty on this value. While the absolute accuracy of the applied protocol could be somewhat challenging [45], it still provides very important insights about the average correlation length of the underlying ordered local distortions.

B. Phase separation

We now turn to the question of phase separation and what our data have to say on this topic. While phase separation with large length-scale domains is clearly dominating in systems with smaller *A*-site ions such as $La_{1-x}Pr_xMnO_3$ [46], for the systems that show robust CMR behavior such as Ca and Sr doped $LaMnO_3$, though the phase separation scenario has been invoked, our results suggest that phase coexistence is minimal in the vicinity of the MI transition at $x \sim 0.2$, at least for the Ca doped state. The rapid crossover from distorted to completely undistorted as the MI transition is crossed, both as a function of T at $x = 0.22$ and as a function of doping x at fixed temperature, would seem to rule out a percolation mechanism for that transition.

Observations of phase separation in these systems from other measurements may be a result of extrinsic effects such as doping or strain, or difficulties in data interpretation [6,14,16,44,47–50].

The situation may be different at higher doping, such as $La_{0.5}Ca_{0.5}MnO_3$ [51], and our results only explicitly address the low-doped region of the phase diagram.

Given the strong electron-phonon coupling and relatively large size of underlying structural distortions in the PI phase, it is sensible to utilize structural signatures of the charge localized and delocalized states to explore the existence and to quantify PS in $La_{1-x}Ca_xMnO_3$. In fact, there was one such attempt in the past from earlier $La_{1-x}Ca_xMnO_3$ PDF experiments [52]. In that study, a two-phase model based on the local structures of the FM and PI phases was used to refine the experimental PDFs quantitatively. The model involved $CaMnO_3$-like undistorted structural phase and $LaMnO_3$-like distorted structural phase with a distortion size associated with the PI component of the order of 0.23 Å (defined as difference between the long and short Mn-O bond) such as seen in the undoped La endmember. Based on the results, a claim was made of the observation of the coexistence of both phases over a wide temperature range. The fits resulted in approximately 10% of the localized JT phase (PI) being present even at the lowest temperature measured (20 K), whereas at room temperature nearly half of the sample remained in the delocalized (FM) phase. However, we note that in this approach to fitting data the quantification of the phase fraction is highly sensitive to the size of the distortion in the distorted PI phase. At the time of that work, the small polaron model was widely accepted for the insulating phase. In this model, the magnitude of the distortion associated with the charge localized Mn^{3+} sites is expected to be as large as that in the $LaMnO_3$ endmember [16,43,44]. However a later, higher resolution, neutron PDF study [26] of the insulating regime of $La_{1-x}Ca_xMnO_3$ revealed that the *local* JT-distortion amplitude in fact decreases dramatically with the increased Ca content, contrary to the small polaron model assumption. This observation calls for the early PDF report of temperature evolution of the phase fraction to be revisited and the phase fraction assignment to be re-examined by a model that uses a more realistic assignment of the underlying local structure of the metallic and insulating phases.

Here we carried out two-phase refinements in a fashion similar to the one described earlier [52] but with the JT distortions set to those observed in the local structure at 10 K for the $x = 0.18$ composition. The structure of the undistorted FM phase was set to that obtained by Rietveld at 10 K for $x = 0.22$ composition. This choice is not optimal as both the average and local structure change with changing the Ca content. However, the changes occurring between $x = 0.18$ and $x = 0.22$ are much smaller than those between $x = 0$ and the doped compositions used [26]. We believe that this assumption is therefore more realistic than the one used in the earlier work [52]. In the two-phase refinements all structural parameters were kept fixed. The only quantities that were allowed to vary were the phase fraction and isotropic correlated ADPs that were constrained to be the same for the two component phases. Typical fits at 10 K are shown in Figs. 6(b) and 6(c). Evolution of the observed undistorted fraction with temperature for the two compositions is presented in Fig. 6(a). No significant contribution of the undistorted phase could be detected in the $x = 0.18$ sample, whose undistorted fraction (and conversely distorted

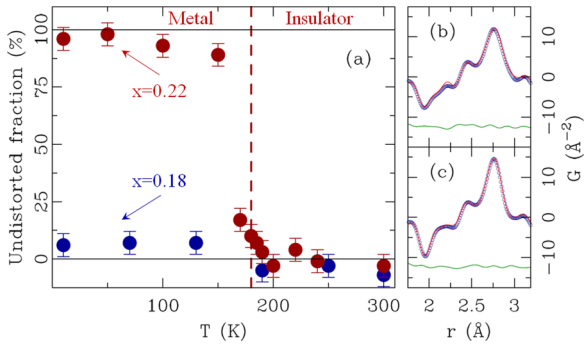

FIG. 6. (a) T evolution of undistorted fraction from two-phase short-range PDF modeling for $x = 0.18$ (solid blue symbols, no MIT), and for $x = 0.22$ (solid red symbols, MIT at ~180 K indicated by a vertical dashed red line). Horizontal solid black lines are guides to the eye. Typical short-range refinements of the two-phase model are shown in (b) for $x = 0.18$ and in (c) for $x = 0.22$ data at 10 K. In both panels open blue symbols represent the data, solid red line is the model, and solid green line is the difference (offset for clarity).

fraction) display almost flat temperature dependence within the accuracy of the assessment. While our analysis cannot unambiguously rule out the existence of phase separation in this composition, it quite strongly suggests that there is virtually no temperature evolution of the local or long-range structure across the temperature range studied, and places an upper limit for undistorted fraction in the $x = 0.18$ sample to below 10%. Similarly, the $x = 0.22$ sample displays almost fully undistorted component in the metallic regime, and fully distorted component in the insulating regime, both displaying no temperature dependence, except in the immediate vicinity of the MI transition. Corresponding correlated ADPs obtained from two-phase fits are shown in Fig. 7(a) (solid symbols) and compared to the uncorrelated values obtained from single phase fits (open symbols). In addition to results for the

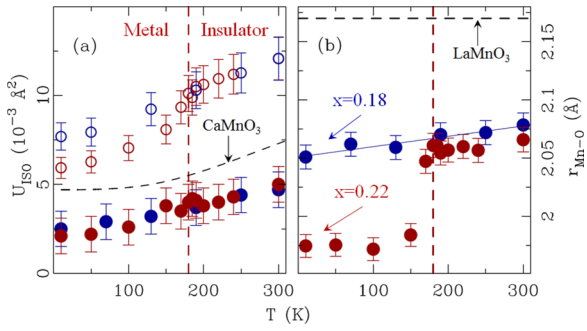

FIG. 7. (a) Comparison of T evolution of uncorrelated ADPs (Rietveld) for $x = 0.18$ (open blue symbols), $x = 0.22$ (open red symbols), and $x = 1.0$ (dashed black line, reference) compositions. Correlated ADPs obtained from two-phase refinements (PDF) are shown by solid symbols for $x = 0.18$ (blue) and $x = 0.22$ (red). (b) Evolution of long Mn-O bond with temperature from short-range PDF modeling. Solid blue symbols represent data for $x = 0.18$ (no MIT), solid red symbols represent data for $x = 0.22$ (MIT at ~180 K, indicated by vertical dashed red line). Horizontal dashed black line marks long Mn-O bond for $x = 0$ (reference) composition. Solid blue line through $x = 0.18$ points is guide to the eye.

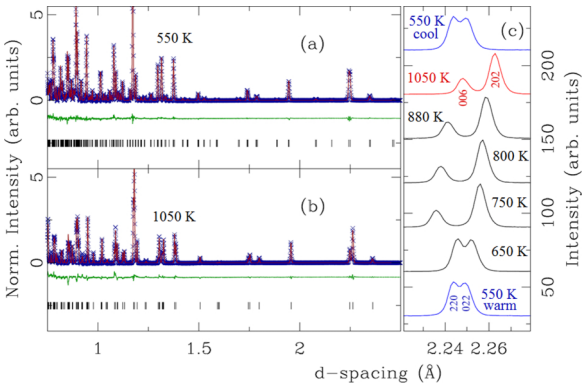

FIG. 8. Rietveld refinements of the average structure models to $La_{1-x}Ca_xMnO_3$ $x = 0.22$ data at (a) 550 K ($Pnma$) and (b) 1050 K ($R\bar{3}c$). Blue symbols represent the data, solid red lines are the model, and solid green lines are the differences (offset for clarity). Vertical ticks mark reflections. (c) Experimental diffraction patterns over a narrow range of d spacing sensitive to O-R average structural transition for temperature as indicated. Profiles have been offset for clarity. The bottom and top profiles correspond to the same 550 K temperature collected on warming and cooling, respectively. Oxygen content refined for these two data sets does not change within the experimental uncertainty, verifying that the sample integrity has been preserved through the heating cycle.

undistorted fraction from two-phase refinements that suggest an abrupt change with no appreciable doping and temperature dependence across the MI transition, changes in uncorrelated ADPs observed in Rietveld refinement, as well as the observed changes in the local long Mn-O bond [Fig. 7(b)], are also abrupt and localized to the immediate vicinity of the transition. The existence of some small amount of residual distorted phase deep in the metallic region, and conversely the existence of some small amount of residual undistorted phase in the insulating region, cannot be ruled out. What is observed here is a dramatic and rapid loss of the distorted Mn octahedra at the MI transition, and relative flatness of the phase fractions away from the transition. This is inconsistent with a picture of the MI transition being percolative in nature, a scenario where the physical properties change rapidly at the transition, but the phase composition evolves slowly through it.

C. High-T behavior: Rhombohedral phase

Finally, we explore the local structure in the high-temperature rhombohedral phase for the $x = 0.22$ sample. Figure 8 shows raw diffraction data and Rietveld refinement fits in this high-temperature region. Understanding nanosale character of orbital correlations has always been a fundamental challenge in CMR systems in general, and in manganites in particular [53]. In $La_{1-x}Ca_xMnO_3$ a systematic study combining high energy x-ray scattering with elastic and inelastic neutron scattering has been employed recently to explore the character of the polaron order and dynamics [54]. It was found that, once established, the nanoscale polaron correlations are only weakly temperature dependent. These short-range correlations were found to have a static component seen in the elastic scattering channel, indicative of the presence of a glasslike state of the polarons, as well as coexisting dynamic correlations with comparable correlation length, as observed by inelastic neutron scattering. It was further established that the elastic component disappears at some characteristic higher temperature T^*, above which the correlations are purely dynamic [54].

The character of nanoscale orbital correlations has been studied at temperatures comparable to the JT transition in $LaMnO_3$ endmember, and at temperatures below the characteristic temperature scale T^*, within what is known as the pseudocubic phase (still $Pnma$ space group) [26,54]. Explorations of orbital correlations in the rhombohedral structural phase at temperatures much higher than both T_{JT} in $LaMnO_3$ and T^* in $La_{1-x}Ca_xMnO_3$ have been scarce. An atomic PDF study explored this temperature regime in the undoped $LaMnO_3$ endmember [23], and found that the local JT distortions persist deep into the rhombohedral phase. Since the PDF method relies indiscriminately on both elastic and inelastic scattering channels, it does not reveal whether the underlying nanoscale orbital correlations are static or dynamic, although it is reasonable to assume that at such high temperature they are probably purely dynamic. Studies of the rhombohedral regime for doped $La_{1-x}Ca_xMnO_3$ samples have been lacking to date. Recent high-resolution synchrotron x-ray powder diffraction measurement explored the existence and character of the rhombohedral phase for $x = 0.3$ composition [38]. A change of polaronic behavior at the pseudocubic ($Pnma$) to rhombohedral ($R\bar{3}c$) structural phase transition (at T_S) from nonadiabatic in the $Pnma$ phase to adiabatic in the $R\bar{3}c$ phase was suggested from resistivity measurements. These results in conjunction with neutron and x-ray studies showing polaron correlations in the orthorhombic phase were interpreted as a scenario in which the structural transition triggers a crossover between distinct electronic states that may be classified as polaron liquid and polaron gas states, though the density of polarons does not change at this transition, so what this picture really means remains unclear.

In order to shed more light on this part of the phase diagram, we explored the evolution of the average and local atomic structure for $x = 0.22$ across the high temperature transition and deep in the $R\bar{3}c$ phase. At this composition T_S is ~720 K. We establish the average structural behavior through Rietveld refinements [Figs. 8(a) and 8(b)], and demonstrate that for the high temperature range studied the sample indeed exhibits the transition where expected. The structural phase transition is clear in the raw diffraction data shown in Fig. 8(c), and the respective Rietveld fits do confirm this [Figs. 8(a) and 8(b)], with data at and above 750 K being in the rhombohedral $R\bar{3}c$ space group. In this space group only a single Mn-O bond distance is allowed, and the temperature dependence of the refined value is shown in Fig. 9(a). It extends continuously from the value in the $Pnma$ model at lower temperature. In that model three distinct distances are allowed; however they refine to almost the same, single value at higher temperatures indicating that on average the MnO_6 octahedra are already approximately regular even before entering the rhombohedral phase. However, close examination of the ADPs [Fig. 9(b)] show that in addition to an anomalous jump in 8d-O ADP temperature dependence at T_{MI}, indicative of the onset of local JT distortions in the insulating phase, there is also a hint of an additional jump, albeit smaller in size, at around T_S,

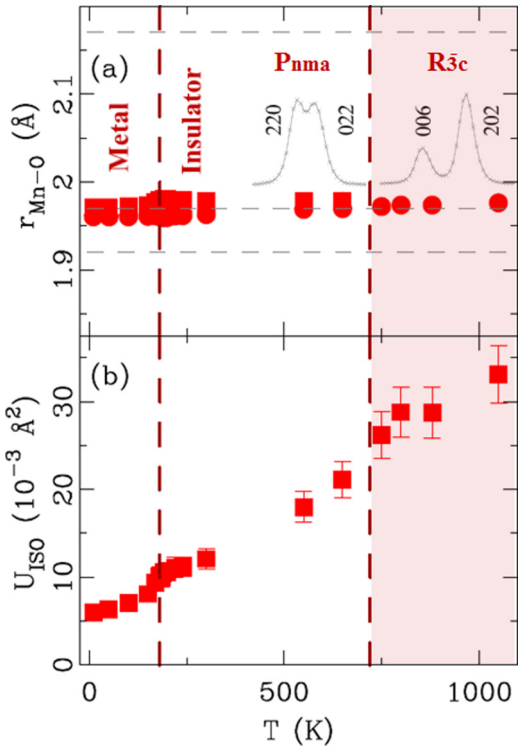

FIG. 9. (a) Temperature evolution of the average Mn-O distances of MnO_6 octahedron for the $x = 0.22$ sample, as obtained from Rietveld refinements across the entire T-range studied. Vertical dashed red lines at ∼180 and ∼720 K mark M-I and O-R transitions, respectively. Vertical dashed lines mark 300 K values for $x = 0$ reference. (b) T evolution of 8d oxygen (*Pnma* model) ADP as obtained from Rietveld refinements. Inset to (a) sketches reflections in the diffraction data characteristic for O and R phases, as shown in Fig. 8(c).

similar to what was observed in $LaMnO_3$ [23]. As discussed earlier, the system below T_S already contains disordered local JT distortions, so this is quite suggestive that the local JT distortions are surviving all the way into the rhombohedral phase, and indeed all the way to our highest temperature data point at 1050 K. This is confirmed in the low-r region of the measured PDFs. Thermal motion of the atoms broaden the PDF peaks making it difficult to resolve clearly the peaks and shoulders directly, but low-r refinements of the PDF clearly prefer distorted MnO_6 octahedra extending to the highest temperatures, as shown in Fig. 10.

PDF analysis shows that JT distortions in $x = 0.22$ persist in the $R\bar{3}c$ phase pretty much in the same fashion as they do in $LaMnO_3$ endmember [23], irrespective of the fact that the JT distortion is crystallographically prohibited. Since the local distortions survive to the highest temperature measured, it is sensible to ask what does in fact change at T_S from the perspective of the local structural footprint of the electronic/orbital state. As was suggested earlier [54], at a characteristic temperature T^* which extends to T_{JT} for $x = 0$ composition ($LaMnO_3$) there is a change from presumably polaron glass (static polarons) below T^* to a polaron liquid (dynamic polarons) above T^*. Since clear JT-distortion signatures persist still above T_S, we suggest that

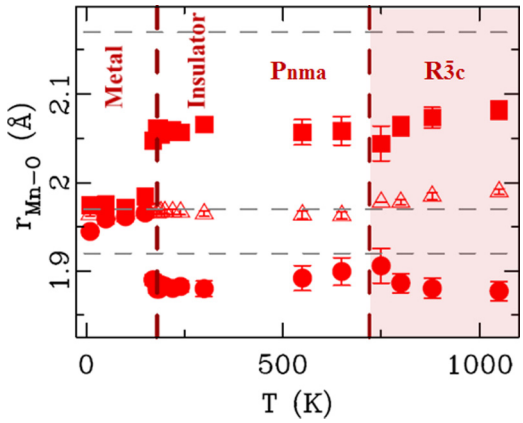

FIG. 10. Temperature evolution of the local Mn-O distances of MnO_6 octahedron for the $x = 0.22$ sample, as obtained from short-range PDF refinements. Local distortions that are onset upon entering the insulating state persist also in the rhombohedral phase, and are seen up to 1050 K—the highest temperature studied. Vertical dashed red lines mark T_{MI} and T_S.

at this point there could be a change in the correlations of the dynamic polarons. At such high temperatures, however, the r-dependent PDF fitting protocol is not so stable due to the thermal broadening of the PDF signal and resulting loss in information in the signal. Instead, we explored an alternative approach (Fig. 11). First, we compare experimental PDFs for $x = 0.22$ at the closest available temperatures bracing the T_S:

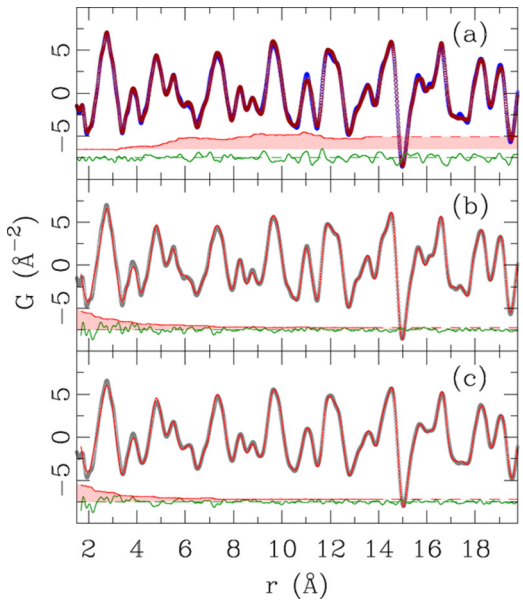

FIG. 11. (a) Comparison of experimental PDF data for $x = 0.22$ at 650 K (*Pnma* phase, open blue symbols) and 750 K ($R\bar{3}c$ phase, open red symbols). (b) and (c) Comparison of the data (open gray symbols) and the *Pnma* model based on intermediate range structure parameters (solid red line) for 650 and 850 K, respectively. In all panels the difference curve (solid green line) is offset for clarity. Light-red solid lines above the differences represent a 4 Å running average of the absolute value of the difference curve, multiplied by 10 and offset for clarity. Shaded areas emphasize the regions of disagreement of the compared PDFs.

650 K data correspond to *Pnma* phase, whereas 750 K data correspond to $R\bar{3}c$ phase, as can be verified from inspecting the respective diffraction patterns shown in Fig. 8(c). This comparison is shown in Fig. 11(a). The difference in the PDFs above and below the transition is captured in the difference curve that is plotted in green below the PDFs. This indicates that the local structure does not change over the length scale of ∼5–6 Å. Further insights can be gained from assessing how well the model that describes the intermediate range PDF data explains the data at low r [45]. To achieve this, a simple two-step procedure was used: in the first step, the PDF data were fit over $10 < r < 20$ Å range; in the second step the structure parameters obtained from the first step were adopted and kept fixed in a refinement of the PDF over $1.7 < r < 20$ Å range, with model parameters that describe correlated motion of nearest neighbors [30] being the only variables. The procedure was applied to 650 K data (below T_S) and 850 K data (above T_S). The resulting fits are shown in Figs. 11(b) and 11(c). The difference curves between the data and the model display behavior inverse of that seen in Fig. 11(a): agreement is good in the high-r region, but poorer at low r, with observable disagreement below ∼6 Å. This not only confirms the existence of local JT distortions in the high temperature regime, but also suggests that the range of correlations of the local JT distortions does not change appreciably on crossing T_S. These observations are in line with previous observations of correlated domain size smoothly changing across T_S in $LaMnO_3$ endmember [23], and also consistent with the change of octahedral rotational degrees of freedom. The PDF approach cannot address the origin or mechanism of the stability of the local distortions. However, it does show very clearly that these distortions do survive up to the highest temperatures, presumably because of Jahn-Teller stabilization energy being very high compared to thermal effects even at these temperatures.

The results of this study suggest that there does not appear to be a broad range of phase coexistence in this material through the MI transition as has been widely thought previously. In contrast, local JT distortions are rapidly suppressed in the metallic phase ($x = 0.22$ at low temperature) on entering both as a function of temperature at fixed doping, or as a function of doping at fixed temperature. These results suggest that the percolative picture for the phase transition is unlikely in our samples. The results are reconciled with earlier PDF studies that suggested otherwise. These studies [16,52] assumed a small-polaron model where the low-r region of the PDF could be rationalized as a mixture of fully JT distorted octahedra and undistorted octahedra. More recent data show that the amplitude of the local JT distortion actually decreases with doping [26] and a simple small polaron scenario is not correct. By taking this into account in the current analysis we obtain a rather different view of the evolution of the metallic and insulating phase fractions with temperature and doping in $La_{1-x}Ca_xMnO_3$. The behavior is different from cubic manganite systems with smaller A-site ions such as $Pr_{1-x}Ca_xMnO_3$ [55,56] where phase coexistence has been clearly established on a longer length scale. On the other hand, the behavior of $La_{1-x}Ca_xMnO_3$ and $La_{1-x}Sr_xMnO_3$ systems are likely to be similar to each other, despite the suggestion of a percolative transition in that system from early PDF data [44]. The persistent feature that was attributed to the Mn-O long bond in that study may have been the feature that we attribute to a termination effect in the current work since it is longer in the doped compounds than the Mn-O long bond in undoped $LaMnO_3$ and not shorter as we now know to be the case.

If the mechanism is not percolative it is interesting to speculate on other mechanisms for the MI transition and CMR effect. A recent in-depth single crystal exploration of the insulating state in the underdoped regime of $La_{1-x}Sr_xMnO_3$ suggested dominant role of superexchange interactions in the ferromagnetic coupling [57]. In this picture orbital mixing alters the interatomic exchange interactions from type-A antiferromagnetic to ferromagnetic order, and can possibly also account for the decrease in the Jahn-Teller oxygen displacements with increasing x, providing a rationale for earlier PDF observations [26]. Such a band model of the σ-bonding $3d$ electrons with magnetic-polaron formation would also be consistent with the current results.

To understand these systems properly, it would be helpful to revisit the $La_{1-x}Sr_xMnO_3$ system using modern experimental and analysis protocols. The behavior of $La_{1-x}Ca_xMnO_3$ at higher dopings could also be understood better, where competition between the metallic and ordered-polaronic charge-ordered phases changes the energy balances and therefore phase coexistence behavior [50,51,58,59].

IV. CONCLUSION

In summary, we have revisited the metal-insulator transition in doped $La_{1-x}Ca_xMnO_3$ ($x = 0.18, 0.22$) with a careful neutron PDF study of the local structure. Distorted MnO_6 octahedra are clearly visible in the local structure wherever the samples are in the polaronic insulating phase. The local JT distortions disappear in the metallic phase. This is in contrast to the observations of the average crystal structure probed either by Rietveld refinement, or refinements of the PDFs carried out over intermediate ranges of r up to 40 Å. Both the correlation length of any ordered JT distortion, and also the phase fraction of metallic and insulating material, have been studied as a function of temperature and doping across the MI transition. We also establish that the local JT distortions persist into the high-temperature rhombohedral phase of the material. The results of the search for phase coexistence show that the undistorted fraction changes abruptly across the MI transition, and the phase fraction stays rather uniform at both sides of the phase line. These observations do not support the percolative scenario for the MI transition in $La_{1-x}Ca_xMnO_3$ and bring the ubiquity of phase separation in the broad class of manganites to question. On the other hand, local distortions of MnO_6 octahedra are found to persist across the pseudocubic to rhombohedral phase transition and deep into the rhombohedral phase where they are crystallographically prohibited.

ACKNOWLEDGMENTS

Work at Brookhaven National Laboratory was supported by U.S. DOE, Office of Science, Office of Basic Energy Sciences (DOE-BES) under Contract DE-SC00112704. Work in the Materials Science Division of Argonne National Laboratory (sample preparation and characterization) was sponsored by

the U.S. Department of Energy Office of Science, Basic Energy Sciences, Materials Science and Engineering Division. Neutron PDF experiments were carried out on NPDF at LANSCE, funded by DOE BES; Los Alamos National Laboratory is operated by Los Alamos National Security LLC under Contract No. DE-AC52-06NA25396. E.S.B. gratefully acknowledges T. E. Proffen and J. Siewenie for assistance with the NPDF measurements.

[1] A. J. Millis, Nature (London) **392**, 147 (1998).
[2] S. Yunoki, A. Moreo, and E. Dagotto, Phys. Rev. Lett. **81**, 5612 (1998).
[3] J.-S. Zhou and J. B. Goodenough, Phys. Rev. B **68**, 144406 (2003).
[4] E. Dagotto, Science **309**, 257 (2005).
[5] N. Bebenin, Phys. Met. Metallogr. **111**, 236 (2011).
[6] M. Uehara, S. Mori, C. H. Chen, and S.-W. Cheong, Nature (London) **399**, 560 (1999).
[7] E. Dagotto, J. Burgy, and A. Moreo, Solid State Commun. **126**, 9 (2003).
[8] J. Burgy, A. Moreo, and E. Dagotto, Phys. Rev. Lett. **92**, 097202 (2004).
[9] E. Dagotto, S. Yunoki, C. Sen, G. Alvarez, and A. Moreo, J. Phys.: Condens. Matter **20**, 434224 (2008).
[10] V. R. Singh, L. Zhang, A. K. Rajapitamahuni, N. Devries, and X. Hong, Phys. Status Solidi **9**, 109 (2012).
[11] D. G. Kuberkar, R. R. Doshi, P. S. Solanki, U. Khachar, M. Vagadia, A. Ravalia, and V. Ganesan, Appl. Surf. Sci. **258**, 9041 (2012).
[12] Z. H. Wu and H. Q. Xie, Physica B **407**, 2538 (2012).
[13] P. Phong, D. Manh, L. Bau, and I.-J. Lee, J. Electroceram. **31**, 364 (2013).
[14] M. Fath, S. Freisem, A. A. Menovsky, Y. Tomioka, J. Aarts, and J. A. Mydosh, Science **285**, 1540 (1999).
[15] J. M. de Teresa, M. R. Ibarra, P. A. Algarabel, C. Ritter, C. Marquina, J. Blasco, J. Garcia, A. del Moral, and Z. Arnold, Nature (London) **386**, 256 (1997).
[16] S. J. L. Billinge, T. Proffen, V. Petkov, J. L. Sarrao, and S. Kycia, Phys. Rev. B **62**, 1203 (2000).
[17] G. Allodi, R. De Renzi, G. Guidi, F. Licci, and M. W. Pieper, Phys. Rev. B **56**, 6036 (1997).
[18] P. A. Kumar, R. Mathieu, P. Nordblad, S. Ray, O. Karis, G. Andersson, and D. D. Sarma, Phys. Rev. X **4**, 011037 (2014).
[19] J. Mitra, M. Paranjape, A. K. Raychaudhuri, N. D. Mathur, and M. G. Blamire, Phys. Rev. B **71**, 094426 (2005).
[20] T. A. Tyson, J. Mustre de Leon, S. D. Conradson, A. R. Bishop, J. J. Neumeier, H. Röder, and J. Zang, Phys. Rev. B **53**, 13985 (1996).
[21] M. F. Hundley, M. Hawley, R. H. Heffner, Q. X. Jia, J. J. Neumeier, J. Tesmer, J. D. Thompson, and X. D. Wu, Appl. Phys. Lett. **67**, 860 (1995).
[22] S. J. L. Billinge, R. G. DiFrancesco, G. H. Kwei, J. J. Neumeier, and J. D. Thompson, Phys. Rev. Lett. **77**, 715 (1996).
[23] X. Qiu, T. Proffen, J. F. Mitchell, and S. J. L. Billinge, Phys. Rev. Lett. **94**, 177203 (2005).
[24] A. Sartbaeva, S. A. Wells, M. F. Thorpe, E. S. Božin, and S. J. L. Billinge, Phys. Rev. Lett. **99**, 155503 (2007).
[25] V. Kiryukhin, New J. Phys. **6**, 155 (2004).
[26] E. S. Božin, M. Schmidt, A. J. DeConinck, G. Paglia, J. F. Mitchell, T. Chatterji, P. G. Radaelli, T. Proffen, and S. J. L. Billinge, Phys. Rev. Lett. **98**, 137203 (2007).
[27] T. Chatterji, F. Fauth, B. Ouladdiaf, P. Mandal, and B. Ghosh, Phys. Rev. B **68**, 052406 (2003).
[28] B. Dabrowski, R. Dybzinski, Z. Bukowski, O. Chmaissem, and J. D. Jorgensen, J. Solid State Chem. **146**, 448 (1989).
[29] M. B. Salamon and M. Jaime, Rev. Mod. Phys. **73**, 583 (2001).
[30] T. Egami and S. J. L. Billinge, *Underneath the Bragg peaks: Structural Analysis of Complex Materials*, 2nd ed. (Elsevier, Amsterdam, 2012).
[31] P. F. Peterson, M. Gutmann, T. Proffen, and S. J. L. Billinge, J. Appl. Crystallogr. **33**, 1192 (2000).
[32] H. M. Rietveld, Acta Crystallogr. **22**, 151 (1967).
[33] A. C. Larson and R. B. Von Dreele, Report No. LAUR-86-748 (1987), Los Alamos National Laboratory, Los Alamos, NM 87545.
[34] B. H. Toby, J. Appl. Crystallogr. **34**, 210 (2001).
[35] C. L. Farrow, P. Juhás, J. Liu, D. Bryndin, E. S. Božin, J. Bloch, T. Proffen, and S. J. L. Billinge, J. Phys.: Condens. Matter **19**, 335219 (2007).
[36] E. S. Božin, A. Sartbaeva, H. Zheng, S. A. Wells, J. F. Mitchell, T. Proffen, M. F. Thorpe, and S. J. L. Billinge, J. Phys. Chem. Solids **69**, 2146 (2008).
[37] Q. Huang, A. Santoro, J. W. Lynn, R. W. Erwin, J. A. Borchers, J. L. Peng, and R. L. Greene, Phys. Rev. B **55**, 14987 (1997).
[38] J. A. Souza, H. Terashita, E. Granado, R. F. Jardim, N. F. Oliveira Jr., and R. Muccillo, Phys. Rev. B **78**, 054411 (2008).
[39] T. Chatterji, B. Ouladdiaf, P. Mandal, B. Bandyopadhyay, and B. Ghosh, Phys. Rev. B **66**, 054403 (2002).
[40] V. Kiryukhin, T. Y. Koo, H. Ishibashi, J. P. Hill, and S. W. Cheong, Phys. Rev. B **67**, 064421 (2003).
[41] V. Kiryukhin, A. Borissov, J. S. Ahn, Q. Huang, J. W. Lynn, and S. W. Cheong, Phys. Rev. B **70**, 214424 (2004).
[42] P. G. Radaelli, M. Marezio, H. Y. Hwang, S. W. Cheong, and B. Batlogg, Phys. Rev. B **54**, 8992 (1996).
[43] C. H. Booth, F. Bridges, G. H. Kwei, J. M. Lawrence, A. L. Cornelius, and J. J. Neumeier, Phys. Rev. Lett. **80**, 853 (1998).
[44] D. Louca, T. Egami, E. L. Brosha, H. Röder, and A. R. Bishop, Phys. Rev. B **56**, R8475(R) (1997).
[45] E. S. Božin, K. R. Knox, P. Juhás, Y. S. Hor, J. F. Mitchell, and S. J. L. Billinge, Sci. Rep. **4**, 4081 (2014).
[46] C. Martin, A. Maignan, M. Hervieu, and B. Raveau, Phys. Rev. B **60**, 12191 (1999).
[47] T. Becker, C. Streng, Y. Luo, V. Moshnyaga, B. Damaschke, N. Shannon, and K. Samwer, Phys. Rev. Lett. **89**, 237203 (2002).
[48] B. M. Ramesh, X. Han, W. Ning, Z.-h. Cheng, Y. Sun, and R. Jayavel, Mater. Lett. **63**, 1528 (2009).
[49] T. Z. Ward, Z. Gai, H. W. Guo, L. F. Yin, and J. Shen, Phys. Rev. B **83**, 125125 (2011).
[50] J. Tao, D. Niebieskikwiat, Q. Jie, M. A. Schofield, L. J. Wu, Q. Li, and Y. M. Zhu, Proc. Natl. Acad. Sci. USA **108**, 20941 (2011).
[51] J. C. Loudon, N. D. Mathur, and P. A. Midgley, Nature (London) **420**, 797 (2002).

[52] T. Proffen and S. J. L. Billinge, Appl. Phys. A **74**, 1770 (2002).
[53] N. Mathur, Nature (London) **390**, 229 (1997).
[54] J. W. Lynn, D. N. Argyriou, Y. Ren, Y. Chen, Y. M. Mukovskii, and D. A. Shulyatev, Phys. Rev. B **76**, 014437 (2007).
[55] Z. Jirák, S. Krupička, Z. Šimša, M. Dlouhá, and S. Vratislav, J. Magn. Magn. Mater. **53**, 153 (1985).
[56] T. Elovaara, H. Huhtinen, S. Majumdar, and P. Patur, J. Phys.: Condens. Matter **26**, 266005 (2014).
[57] J.-S. Zhou and J. B. Goodenough, Phys. Rev. B **91**, 064414 (2015).
[58] T. Wu, S. B. Ogale, J. E. Garrison, B. Nagaraj, A. Biswas, Z. Chen, R. L. Greene, R. Ramesh, T. Venkatesan, and A. J. Millis, Phys. Rev. Lett. **86**, 5998 (2001).
[59] J. Tao, D. Niebieskikwiat, M. B. Salamon, and J. M. Zuo, Phys. Rev. Lett. **94**, 147206 (2005).